bio-protocol

Open Access

Published: **Apr 05, 2023**

Reconstitution of Membrane-tethered Postsynaptic Density Condensates Using Supported Lipid Bilayer

Zhe Feng[1, *] and Mingjie Zhang[2]

[1]State Key Laboratory of Genetic Engineering, School of Life Sciences, Fudan University, Shanghai, 200433, China
[2]School of Life Sciences, Southern University of Science and Technology, Shenzhen 518055, China
*For correspondence: zhefeng@fudan.edu.cn

Abstract

Eukaryotic cells utilize sub-cellular compartmentalization to restrict reaction components within a defined localization to perform specified biological functions. One way to achieve this is via membrane enclosure; however, many compartments are not bounded with lipid membrane bilayers. In the past few years, it has been increasingly recognized that molecular components in non- or semi-membrane-bound compartments might form biological condensates autonomously (i.e., without requirement of energy input) once threshold concentrations are reached, via a physical chemistry process known as liquid–liquid phase separation. Molecular components within these compartments are stably maintained at high concentrations and separated from the surrounding diluted solution without the need for a physical barrier. Biochemical reconstitution using recombinantly purified proteins has served as an important tool for understanding organizational principles behind these biological condensates. Common techniques include turbidity measurement, fluorescence imaging of 3D droplets, and atomic force microscopy measurements of condensate droplets. Nevertheless, many molecular compartments are semi-membrane-bound with one side attached to the plasma membrane and the other side exposed to the cytoplasm and/or attached to the cytoskeleton; therefore, reconstitution in 3D solution cannot fully recapture their physiological configuration. Here, we utilize a postsynaptic density minimal system to demonstrate that biochemical reconstitution can be applied on supported lipid bilayer (SLB); we have also incorporated actin cytoskeleton into the reconstitution system to mimic the molecular organization in postsynaptic termini. The same system could be adapted to study other membrane-proximal, cytoskeleton-supported condensations.

Keywords: Phase separation, Synapses, Biochemical reconstitution, Supported lipid bilayer, Actin cytoskeleton

This protocol was validated in: J Cell Biol (2022), DOI: 10.1083/jcb.202105035

Background

Neurons communicate via synapses that constitute the presynaptic bouton, synaptic cleft, and postsynaptic termini. Postsynaptic density (PSD) refers to a densely packed, protein-enriched area that locates just beneath the postsynaptic membrane. It contains thousands of proteins such as transmembrane receptors and channels, scaffold proteins, protein kinases and other enzymes, and cytoskeletal proteins. PSD serves as a signaling hub that converges signals received from the presynaptic termini and translates them into a series of downstream cellular processes, including dynamic translocation of receptors, re-organization of actin cytoskeleton, and regulation of protein degradation machinery, ultimately leading to altered synaptic morphology and function. The tiny compartmental size of neuronal synapses, the great heterogeneity across synapses, and the redundancy and compensation between different signaling pathways all make it more challenging to investigate mechanistic details behind synaptic organization via conventional imaging techniques. Recent studies have suggested that phase separation might provide an explanation to how synaptic compartments, including the presynaptic active zone and PSD, are assembled (Zeng et al., 2016, 2018 and 2019; Milovanovic et al., 2018; Wu et al., 2019 and 2021; McDonald et al., 2020; Pechstein et al., 2020; Bai et al., 2021; Cai et al., 2021; Hosokawa et al., 2021). In previously published studies, we demonstrated that major excitatory PSD (ePSD) scaffold proteins, when mixed in vitro, could readily condense into molecular assemblies via phase separation (Zeng et al., 2018; Feng et al., 2022). This minimal ePSD system reconstituted in vitro is reminiscent of the ePSD assemblies in vivo in many aspects. ePSD condensates could cluster receptors, exclude inhibitory PSD proteins, and be dispersed in the presence of negative regulators. The biochemically reconstituted minimal PSD system, therefore, provides a powerful platform to bridge in vitro observations to cellular functions in vivo. To better mimic the physiological context of semi-membrane-tethered ePSD assemblies, we developed methods for reconstituting microclusters using purified proteins assembled on supported lipid bilayers (SLBs) (Feng et al., 2022). We attached PSD-95 through the interaction of N-terminal His8 tag with Ni-NTA-functionalized lipids incorporated into the bilayer in order to mimic its membrane proximal localization via N-terminal palmitoylation in a physiological context. We also incorporated phosphatidylinositol 4,5-bisphosphate [PI (4,5) P2] lipids into the bilayer to enable insulin receptor substrate protein 53 (IRSp53), a major PSD scaffold protein as well as a PIP2 binder, to localize to the membrane via its Bin/Amphiphysin/RVS (BAR) domain known to bind negatively charged lipids. To enable visualization, we labeled proteins with amide/maleimide-conjugated fluorophores. PSD-95 was uniformly distributed on membranes and readily assembled into nanodomains when other PSD scaffold proteins, SH3 and multiple ankyrin repeat domains 3 (Shank3), guanylate kinase–associated protein (GKAP), IRSp53, and Homer3, were added to trigger phase separation. We incubated all the components with actin in the experimental system. We observed that rhodamine-labeled actin co-localized with the PSD condensates on the membrane and formed thin filament bundles. This reconstitution system allows us to investigate interactions between lipid membranes, membrane-proximal molecular assemblies, and actin cytoskeleton, as well as to recapture complex cellular behaviors observed in vivo.

Materials and Reagents

1. Proteins: PSD-95, IRSp53, Shank3, GKAP, and Homer3 [see Feng et al. (2022) for protein production details]
2. Rabbit skeletal muscle actin (Cytoskeleton, Inc., catalog number: AKL99), rhodamine actin from rabbit skeletal muscle (Cytoskeleton, Inc., catalog number: AR05)
3. Lipid components:
   1-palmitoyl-2-oleoyl-sn-glycero-3-phosphocholine (POPC) (Avanti, catalog number: 850457P)
   1,2-dioleoyl-sn-glycero-3-phospho-(1’-myo-inositol-4’,5’-bisphosphate) [18:1 PI (4,5) P2] (Avanti, catalog number: 850155P)
   1,2-dioleoyl-sn-glycero-3-[(N-(5-amino-1-carboxypentyl) iminodiacetic acid) succinyl] (DGS-NTA) (Avanti, catalog number: 790404P)
   1,2-dioleoyl-sn-glycero-3-phosphoethanolamine-N-[methoxy(polyethylene glycol)-5000] (PEG5000PE) (Avanti, catalog number: 880230P)
4. Fluorophores:

Alexa Fluor™ 647 NHS ester (Thermo Fisher, catalog number: A20006)
Cy3® NHS ester (AAT Bioquest, catalog number: 271)
Alexa Fluor™ 488 C_5 maleimide (Thermo Fisher, catalog number: A10254)
DiO perchlorate (AAT Bioquest, catalog number: 22066)

5. Chambered cover glass (Lab-tek®, catalog number: 155409)
6. Amber glass vials (Thermo Fisher, catalog number: B7800-1-9A)
7. Hellmanex III (Helma Analytics™, catalog number: Z805939)
8. Gastight syringes [Agilent, catalog numbers: 5190-1471 (2 µL), 5190-1483 (10 µL), 5190-1493 (25 µL), and 5190-1507 (100 µL)]
9. Chloroform (Scharlab, product code: 10289473)
10. NaOH (Scharlab, catalog number: SO04251000)
11. Sodium cholate (Sigma, catalog number: 27029)
12. BSA (Goldbio, catalog number: A-421-500)
13. ATP (Sigma, product number: A6144)
14. $MgCl_2$ (VWR Chemicals BDH®, catalog number: BDH9244)
15. NaH_2PO_4 (Millipore, catalog number: 567545)
16. KH_2PO_4 (Sigma, catalog number: P0662)
17. NaCl (Santa Cruz Biotechnology®, catalog number: SC-203274)
18. KCl (VWR Chemicals BDH®, catalog number: 26764)
19. Tris-HCl (Goldbio, catalog number: T-400-5)
20. DL-Dithiothreitol (DTT) (Sigma, catalog number: D0632)
21. $CaCl_2$ (Sigma, catalog number: C4901)
22. HiTrap desalting column (Cytiva, catalog number: 89501-384)
23. PBS buffer (see Recipes)
24. Reaction buffer (see Recipes)
25. G-buffer (see Recipes)

Equipment

1. Water bath (Shel lab, model number: 1201-2E)
2. Oven incubator (Binder GmbH, art number: 9010-0002)
3. High-speed centrifuge (Eppendorf, catalog number: 540600097)
4. AKTApurifier (GE Healthcare, USA)
5. Zeiss LSM 800 microscope (Zeiss)
6. Nanodrop

Software

1. FIJI (ImageJ)

Procedure

A. Preparation of small unilamellar vesicles (SUV)

1. Warm up individual lipid stocks (dissolved in chloroform) to room temperature.
2. Use glass syringe (see Materials and Methods for details of syringes used here) to prepare lipid mixture with the following composition: 95.9% POPC, 2% DGS-NTA (Ni), 2% PI (4,5) P2, and 0.1% PEG5000PE.

Mix the following components in a glass vial:

POPC (13.16 mM stock)	7.1 µL
DGS-NTA (Ni) (4.74 mM stock)	0.42 µL
PIP2 (500 µM stock)	3.9 µL
PEG5000PE (170 µM stock)	0.57 µL

Note that the above lipid quantities are calculated to coat a single cover glass well (i.e., 75 µg total).

3. Dry the lipid mix under a stream of nitrogen gas with rotation. You will see multiple white layers adhered to the wall of the vial after the lipids are dried (Figure 1). Note that 1% DiO perchlorate dye is included to label the lipids for a better visualization in Figure 1.

Figure 1. Image showing dried lipid layers adhered to the wall of a glass vial. 1% DiO dye is included to label the lipids for better demonstration.

4. Continue to dry the lipids under vacuum for at least 1 h to ensure removal of residual chloroform.
5. Resuspend the lipid mixture with vigorous pipetting and vortexing in ≤300 µL (the resuspension volume/the column injection volume is determined by the column resolution) of PBS buffer supplemented with 1% v/v sodium cholate. Lipids should be completely transparent once fully dissolved in detergent-containing buffer.
6. Subject the dissolved lipid mixture to a HiTrap desalting column equilibrated with the detergent-free PBS buffer. Use an FPLC system and pool fractions with detected UV absorbance at 280 nm, followed by dilution to the desired volume with PBS buffer. Add 150 µL of lipid solution to coat each well glass to generate SLBs.

B. Preparation of supported lipid bilayers (SLBs)

1. Wash the chambered cover glass (well area of 0.7 cm^2) with 5% Hellmanex III overnight at room temperature and thoroughly rinse with Milli-Q water the next morning.
2. Wash the cover glass with 5 M NaOH for 1 h at 50 ℃ and then rinse thoroughly with Milli-Q water. Repeat this wash step three times.
3. To each cleaned cover glass, add 500 µL of PBS buffer for equilibration, take out, and discard.
4. Add 150 µL of SUVs to each cover glass well and incubate for 1 h at 42 ℃ to generate SLBs.
5. Wash the SLBs with 750 µL of reaction buffer three times to achieve 216-fold dilution. It should be noted that SLBs should not be exposed to the atmosphere to prevent oxidation.
6. Block the SLBs with 1 mg/mL BSA (stock concentration of 100 mg/mL) in the reaction buffer at room temperature for 30 min.
7. Add 2 µM 10% Alexa 647- or Cy3-labeled, His8-tagged PSD-95 protein to the SLBs and leave for incubation with SLBs for 1 h at room temperature.
8. Wash away the unbound His-PSD-95 with the reaction buffer three times (750 µL per wash).
9. Image using Zeiss LSM 800 microscope (Figure 2Ai).

C. Imaging membrane localization of PIP2 binder

1. Add 1 μM 10% Alexa 488–labeled IRSp53 protein to the SLBs and leave for incubation with SLBs for 1 h at room temperature.
2. Wash the SLBs with the reaction buffer three times (750 μL per wash) to remove any unbound IRSp53 protein.
3. Image using Zeiss LSM 800 microscope (Figure 2Aii).

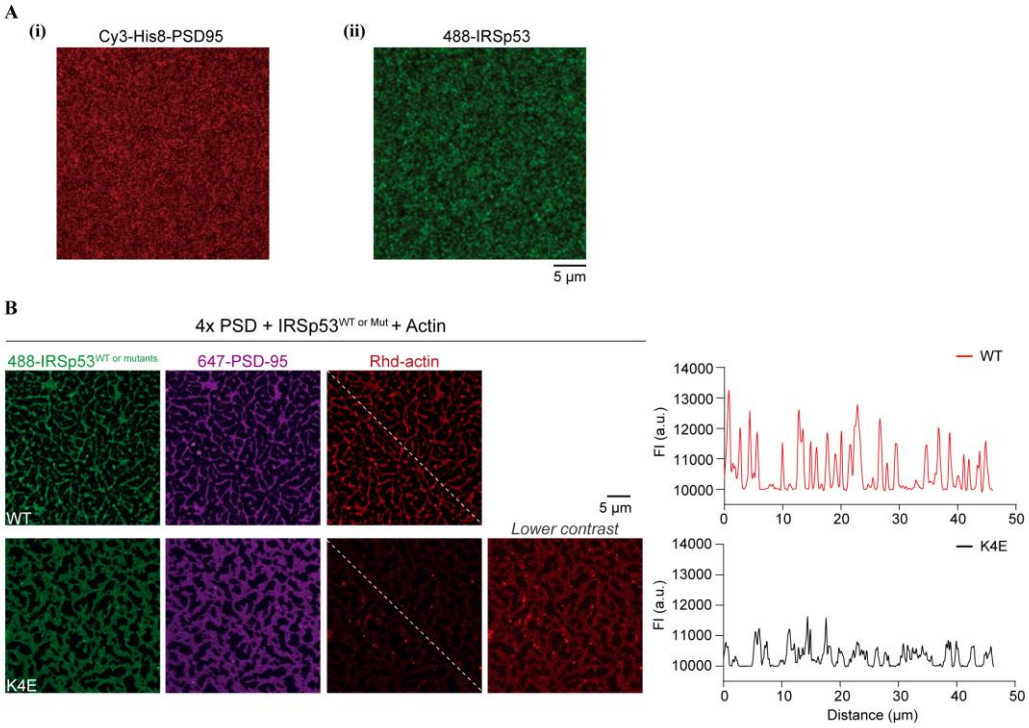

Figure 2. Postsynaptic density (PSD) condensation and actin polymerization on supported lipid bilayers (SLBs). (A) Fluorescence images showing uniform coating of Cy3-labeled, His8-tagged PSD-95 (i) or Alexa 488–labeled IRSp53 (ii) on SLBs before the addition of other PSD scaffold proteins. **(B)** Representative fluorescence images showing actin filaments assembled from PSD condensates on the SLB. An actin-binding-deficient mutant of IRSp53 (K4E) shows significantly diminished actin bundling to PSD condensates on the membrane. A line plot of the rhodamine-labeled actin intensities along the dashed line is presented. Figures are adapted from Feng et al. (2022) with permission.

D. Actin reconstitution and labeled actin preparation

1. Reconstitute lyophilized muscle actin protein to 10 mg/mL with 100 μL of deionized water and then dilute to 0.4 mg/mL in G-buffer supplemented with 0.2 mM ATP and 0.5 mM DTT.
2. After reconstitution, incubate actin on ice for 1 h to depolymerize actin oligomers that form during storage. Further centrifuge the actin resuspension at 14,000 × *g* for 15 min at 4 ℃.
3. Transfer the supernatant to a new microcentrifuge tube and determine the total protein concentration with a NanoDrop.
4. Reconstitute lyophilized rhodamine muscle actin protein to 10 mg/mL with 2 μL of deionized water and then dilute to 2 mg/mL with G-buffer supplemented with 0.2 mM ATP and 1 mM DTT.
5. Leave actin solution on ice for 1 h to depolymerize actin oligomers.
6. Centrifuge the rhodamine actin resuspension at 14,000 × *g* for 15 min at 4 ℃.

7. Transfer the top 90% of the supernatant to a new tube and determine the total protein concentration and percentage of rhodamine-labeled protein with a NanoDrop.

E. Imaging microcluster formation and actin polymerization

1. Premix 250 nM of Shank3, GKAP, Homer3, and IRSp53, as well as 1 μM of 10% rhodamine-labeled actin in reaction buffer supplemented with 1 mM ATP and 2 mM $MgCl_2$. The total solution volume in each chambered glass well is 150 μL.
2. Add the pre-mixture to the Alexa 647–labeled His8-PSD-95-bound SLBs and incubate for 20 min to allow microcluster formation and actin polymerization on the membrane.
3. Image using Zeiss LSM 800 microscope. Actin polymerization occurs within 20 min after mixture and reaches a plateau after 1 h. All data should be collected within 8 h after lipid coating started.

Data analysis

Analyzing actin recruitment with FIJI (ImageJ)

1. Open the captured image using FIJI.
2. To analyze actin enrichment within membrane localized clusters, draw a diagonal line across the image and measure the fluorescence intensity by Plot Profile. Note that it is essential to use identical imaging settings for direct comparison between different experiments.

Recipes

1. PBS buffer

10 mM NaH_2PO_4/1.8 mM KH_2PO_4, pH 7.4
137 mM NaCl
27 mM KCl

2. Reaction buffer

50 mM Tris-HCl, pH 8.0
100 mM NaCl
2 mM DTT

3. G-buffer

5 mM Tris-HCl, pH 8.0
0.2 mM $CaCl_2$
0.2 mM ATP

Acknowledgments

This work was supported by grants from the Ministry of Science and Technology of China (2019YFA0508402), the National Science Foundation of China (82188101), Research Grants Council (RGC) of Hong Kong (AoE-M09-12, 16104518 and 16101419), a Human Frontier Science Program research grant (RGP0020/2019) to M. Zhang, and an RGC General Research Fund (GRF) grant (16102120) to Z. Feng. The protocol was adapted from Feng et al. (2022).

Competing interests

The authors declare no competing interests.

References

Bai, G., Wang, Y. and Zhang, M. (2021). Gephyrin-mediated formation of inhibitory postsynaptic density sheet via phase separation. *Cell Res* 31(3): 312-325.

Cai, Q., Zeng, M., Wu, X., Wu, H., Zhan, Y., Tian, R. and Zhang, M. (2021). CaMKIIalpha-driven, phosphatase-checked postsynaptic plasticity via phase separation. *Cell Res* 31(1): 37-51.

Feng, Z., Lee, S., Jia, B., Jian, T., Kim, E. and Zhang, M. (2022). IRSp53 promotes postsynaptic density formation and actin filament bundling. *J Cell Biol* 221(8): e202105035.

Hosokawa, T., Liu, P. W., Cai, Q., Ferreira, J. S., Levet, F., Butler, C., Sibarita, J. B., Choquet, D., Groc, L., Hosy, E., et al. (2021). CaMKII activation persistently segregates postsynaptic proteins via liquid phase separation. *Nat Neurosci* 24(6): 777-785.

McDonald, N. A., Fetter, R. D. and Shen, K. (2020). Assembly of synaptic active zones requires phase separation of scaffold molecules. *Nature* 588(7838): 454-458.

Milovanovic, D., Wu, Y., Bian, X. and De Camilli, P. (2018). A liquid phase of synapsin and lipid vesicles. *Science* 361(6402): 604-607.

Pechstein, A., Tomilin, N., Fredrich, K., Vorontsova, O., Sopova, E., Evergren, E., Haucke, V., Brodin, L. and Shupliakov, O. (2020). Vesicle Clustering in a Living Synapse Depends on a Synapsin Region that Mediates Phase Separation. *Cell Rep* 30(8): 2594-2602 e2593.

Wu, X., Cai, Q., Shen, Z., Chen, X., Zeng, M., Du, S. and Zhang, M. (2019). RIM and RIM-BP Form Presynaptic Active-Zone-like Condensates via Phase Separation. *Mol Cell* 73(5): 971-984 e975.

Wu, X., Ganzella, M., Zhou, J., Zhu, S., Jahn, R. and Zhang, M. (2021). Vesicle Tethering on the Surface of Phase-Separated Active Zone Condensates. *Mol Cell* 81(1): 13-24 e17.

Zeng, M., Chen, X., Guan, D., Xu, J., Wu, H., Tong, P. and Zhang, M. (2018). Reconstituted Postsynaptic Density as a Molecular Platform for Understanding Synapse Formation and Plasticity. *Cell* 174(5): 1172-1187. e16.

Zeng, M., Diaz-Alonso, J., Ye, F., Chen, X., Xu, J., Ji, Z., Nicoll, R. A. and Zhang, M. (2019). Phase Separation-Mediated TARP/MAGUK Complex Condensation and AMPA Receptor Synaptic Transmission. *Neuron* 104(3): 529-543 e526.

Zeng, M., Shang, Y., Araki, Y., Guo, T., Huganir, R. L. and Zhang, M. (2016). Phase Transition in Postsynaptic Densities Underlies Formation of Synaptic Complexes and Synaptic Plasticity. *Cell* 166(5): 1163-1175. e12.